

**Joule, Volume 7**

**Supplemental information**

**Oxide layer coating enabling oxysulfide-based  
photocatalyst sheet to drive Z-scheme  
water splitting at atmospheric pressure**

**Swarnava Nandy, Takashi Hisatomi, Mamiko Nakabayashi, Huihui Li, Xiaojun Wang, Naoya Shibata, Tsuyoshi Takata, and Kazunari Domen**

## Supplemental Experimental Procedures:

### 1. Synthesis of photocatalysts

#### 1.1. Synthesis of doped $\text{La}_5\text{Ti}_2\text{Cu}_{0.9}\text{Ag}_{0.1}\text{O}_7\text{S}_5$ photocatalysts:

Mg, Al codoped  $\text{La}_5\text{Ti}_2\text{Cu}_{0.9}\text{Ag}_{0.1}\text{O}_7\text{S}_5$  (LTCA:Mg, Al) was synthesized by a solid-state reaction (SSR).  $\text{Mg}(\text{NO}_3)_2 \cdot 6\text{H}_2\text{O}$  (99.5%, Fujifilm Wako Pure Chemical Co.) and  $\text{Al}(\text{NO}_3)_3 \cdot 9\text{H}_2\text{O}$  (99.5%, Fujifilm Wako Pure Chemical Co.) as Mg and Al dopant sources, respectively, were first impregnated onto  $\text{TiO}_2$  (rutile, 99.99%, Kanto Chemical Co. Inc.) and calcined at 1073 K for 1 h in air. The  $\text{Mg}/(\text{Mg}+\text{Al}+\text{Ti})$  and  $\text{Al}/(\text{Mg}+\text{Al}+\text{Ti})$  molar ratios were both 1%. The resulting material is denoted as  $\text{TiO}_2(\text{Mg, Al})$ .  $\text{La}_2\text{O}_3$  (99.99%, Kanto Chemical Co., Inc.) was calcined in air at 1273 K for 10 h to remove moisture and carbonate before mixing.  $\text{La}_2\text{O}_3$ ,  $\text{La}_2\text{S}_3$  (99.9%, Kojundo Chemical Laboratory Co., Ltd.),  $\text{TiO}_2(\text{Mg, Al})$ ,  $\text{Cu}_2\text{S}$  (99%, Kojundo Chemical Laboratory Co., Ltd.),  $\text{Ag}_2\text{S}$  (99%, Kojundo Chemical Laboratory Co., Ltd.) and sulfur (99.99%, Kojundo Chemical Laboratory Co., Ltd.) were mixed at a  $\text{La}_2\text{O}_3:\text{La}_2\text{S}_3:\text{TiO}_2(\text{Mg, Al}):\text{Cu}_2\text{S}:\text{Ag}_2\text{S}:\text{S}$  molar ratio of 2:3:4:0.9:0.1:0.25 in a nitrogen filled glovebox. The precursor mixtures were sealed in evacuated quartz tubes and heated from room temperature to 473 K in 9 min, from 473 to 673 K in 100 min, and from 673 to 1323 K in 53 h, and then maintained at 1323 K for 96 h. After the termination of the annealing process, the solid chunk thus produced was ground into powder. Ga-doped LTCA was also synthesized by SSR. An accurate amount of  $\text{Ga}_2\text{O}_3$  (99.5% Fujifilm Wako Pure Chemical Co.) was included in the precursor mixture and an equivalent amount of  $\text{TiO}_2$  was reduced. The  $\text{Ga}/(\text{Ga}+\text{Ti})$  molar ratio was 1%.

#### 1.2. Synthesis of Mo-doped $\text{BiVO}_4$ (BVO:Mo) photocatalysts:

Mo-doped  $\text{BiVO}_4$  (BVO:Mo, Mo/V = 0.1 mol%) was synthesized by solid-liquid (s-l) and hydrothermal (h) reaction methods according to previous studies.<sup>S1,S2</sup> For the preparation of BVO:Mo (s-l), a mixture of  $\text{K}_2\text{CO}_3$  ( $\geq 99.5\%$ , Kanto Chemical Co. Inc.),  $\text{MoO}_3$  ( $\geq 99.0\%$ , Kanto Chemical Co. Inc.), and  $\text{V}_2\text{O}_5$  ( $\geq 99.0\%$ , Wako Pure Chemical Industries, Ltd.) was prepared and calcined in air at 723 K for 5 h to prepare Mo-doped  $\text{K}_3\text{V}_5\text{O}_{14}$  ( $\text{K}_3\text{V}_5\text{O}_{14}:\text{Mo}$ ). An aqueous suspension was prepared by dispersing  $\text{Bi}(\text{NO}_3)_3 \cdot 5\text{H}_2\text{O}$  ( $\geq 99.9\%$ , Kanto Chemical Co. Inc.) in distilled water. The prepared  $\text{K}_3\text{V}_5\text{O}_{14}:\text{Mo}$  powder was added to this suspension, and the suspension was stirred at 70°C for 10 h. The resulting yellow BVO:Mo sample was collected after washing with distilled water followed by drying in an oven overnight at 313 K.

For the synthesis of BVO:Mo (h), the precursors  $\text{NH}_4\text{VO}_3$  (99.0%, Fujifilm Wako Pure Chemical Co.) (5 mmol),  $\text{Bi}(\text{NO}_3)_3 \cdot 5\text{H}_2\text{O}$  (5 mmol) and  $\text{MoO}_3$  were added to 60 mL of a 2 M  $\text{HNO}_3$  solution in a beaker. The pH of the solution was adjusted to 0.5 by adding an ammonia aqueous solution (25 wt%, Fujifilm Wako Pure Chemical Co.) while stirring. After continuous stirring for 2 h, the light-yellow precipitate in the beaker was transferred to a 100 mL Teflon-lined stainless-steel autoclave and hydrothermally treated at 473 K for 12 h. After the autoclave cooled to room temperature, the vivid yellow colored powder was separated by filtration and washed with distilled water several times. Then, the powder was dried at 313 K overnight.

### 2. Fabrication of photocatalyst sheets and photoelectrodes:

Photocatalyst sheets were fabricated by a particle transfer method as in previous studies.<sup>S1,S3</sup> The LTCA:Mg, Al and BVO:Mo photocatalysts (10 mg each) were suspended in 0.5 mL of isopropanol, ultrasonicated for several minutes and drop-casted onto a clean 3×3 cm glass plate. After drying overnight, a thin layer of Au with a thickness of 0.3 μm was deposited by vacuum evaporation (VFR-200 M/ERH, ULVAC KIKO, Inc.) at a deposition rate of 7–8 nm s<sup>-1</sup>. The resulting sample was then heated at 523 K for 10 min to reduce the contact resistance between the semiconductor particles and the Au contact layer. In some cases, a C layer with a thickness of 0.3 μm was deposited by direct current magnetron sputtering (ES-250L, Eiko Engineering, Co., Ltd.) in an Ar atmosphere with a background pressure of 0.5 Pa for 2.5 h at 75 W. After that, the primary glass plate was attached to a second glass substrate covered with adhesive carbon tape (Nisshin EM Co., Ltd.) to transfer the photocatalysts and Au layer. Loosely-bound particles were removed from the sample by ultrasonication three times for a few seconds exchanging the distilled water each time.

LTCA:Mg,Al, LTCA:Ga, and BVO:Mo photoelectrodes were also fabricated by a particle transfer method.<sup>S4</sup> Au was employed as a back contact material to simulate an environment identical to that for the photocatalyst sheet system. A Au layer 2 μm in thickness was deposited by vacuum evaporation onto 3×3 cm glass substrates coated with LTCA:Ga, LTCA:Mg,Al, BVO:Mo(h), and BVO:Mo(s-l) powders. After deposition of Au, the samples were heated at 523 K for 10 min. Electrical contact was established by connecting a Cu wire to the Au layer using indium solder. Finally, the Cu wire and indium solder were covered with epoxy resin.

Au electrodes were fabricated to examine the oxygen reduction reaction (ORR) activity of a bare gold electrode as a reference. Au layer was deposited on a titanium plate (1×1 cm) to a thickness of 0.3 μm by vacuum evaporation. Electrical contact was established by connecting a Cu wire using indium solder at the rear side of the electrode, followed by covering with epoxy resin.

### **3. Loading of cocatalysts and surface modifiers:**

#### **3.1. Cocatalysts loading:**

Rh cocatalysts was deposited onto the photocatalyst sheet (9 cm<sup>2</sup>) by a two-step adsorption-nucleation and photodeposition method following our recent study on LTCA:Ga/Au/BVO:Mo(s-l) sheets.<sup>S5</sup> Briefly, Rh particles were adsorbed on a bare LTCA:Mg,Al/Au/BVO:Mo sheet sample by immersing it in a 45 μM aqueous RhCl<sub>3</sub> solution for 2 h under darkness. The solution was then exchanged with fresh distilled water and the sheet was irradiated under visible light for 1 h. After Rh adsorption and nucleation, 0.1 μmol of Rh was additionally photodeposited from RhCl<sub>3</sub> on to a photocatalyst sheet in distilled water for 1.5 h. After that, the reaction solution was exchanged with fresh distilled water containing 0.2 μmol K<sub>2</sub>CrO<sub>4</sub>, and Cr<sub>2</sub>O<sub>3</sub> was photodeposited for 2 h to form the Cr<sub>2</sub>O<sub>3</sub> shell-Rh core cocatalyst. CoO<sub>x</sub> (0.05 μmol) was also photodeposited as an oxygen evolution cocatalyst after loading the Cr<sub>2</sub>O<sub>3</sub>/Rh cocatalyst for 1 h. The photodeposition reactions were carried out in 40 mL of distilled water under visible light irradiation ( $\lambda > 420$  nm) from a Xe lamp in a closed circulation system.

#### **3.2. TiO<sub>2</sub> coating:**

An amorphous TiO<sub>2</sub> layer was deposited onto the photocatalyst sheet by photodecomposition of titanium peroxide.<sup>S6</sup> A titanium peroxide solution was prepared by adding 10 μL

of titanium tetraisopropoxide (TTIP) ( $\geq 97\%$ , Kanto Chemical Co. Inc.) and 20  $\mu\text{L}$  of  $\text{H}_2\text{O}_2$  ( $\geq 30\%$ , Fujifilm Wako Pure Chemical Co.) to 1 mL of distilled water. Then, the resulting suspension of TTIP/ $\text{H}_2\text{O}_2$  was sonicated for several minutes until it changed into a transparent yellow solution. A certain amount of the solution was added to 40 mL of distilled water in which the sheet sample was submerged. The photodecomposition reaction was then conducted using a closed circulation system under irradiation from a 300 W Xe lamp ( $\lambda > 420 \text{ nm}$ ) for 2 h. The amount of  $\text{TiO}_2$  was varied in the range of 0.26–1.6 mg. Note that oxygen gas was predominately evolved for the first few hours under irradiation owing to the decomposition of the peroxide species.

### 3.3. $\text{SiO}_2$ coating:

An  $\text{SiO}_2$  layer was deposited from tetraethyl orthosilicate (TEOS) ( $>97\%$ , Tokyo Chemical Industry Co., Ltd.) by hydrolysis. TEOS (20–40  $\mu\text{L}$ ) was mixed with distilled water (50  $\mu\text{L}$ ). The solution was allowed to rest for 1 h, then dispersed (by ultrasonication for 1 min), and immediately drop-casted using a micropipette onto the cocatalyst-modified sheet (9  $\text{cm}^2$ ) with varying volumes (20–40  $\mu\text{L}$ , corresponding to 5.4–10.8 mg of  $\text{SiO}_2$  nominally). The sample was immersed in 40 mL of distilled water after being left in air at room temperature for 20 min.

## 4. Z-scheme overall water splitting reaction:

A closed gas-circulation system was used to evaluate the Z-scheme overall water splitting (ZOWS) activity of cocatalyst-modified LTCA:Mg,Al/Au/BVO:Mo sheets. Photocatalyst sheet samples (9  $\text{cm}^2$ ) were placed at the bottom of a top-irradiation type reactor made of Pyrex glass, and 40 mL of distilled water without pH adjustment was added to the reactor. The reactor was evacuated thoroughly to remove air. Unless otherwise noted, the reaction temperature was maintained at approximately 283 K using a flow of cooling water. In most trials, the reaction was conducted without introducing Ar, and the initial pressure in the reaction system was 2 kPa. The gas evolution activity of the photocatalyst sheet was examined as a function of the initial background pressure by introducing Ar in the range of 2–90 kPa into the closed gas-circulation system. The activity was also measured at different reaction solution temperatures ranging from 283 to 333 K. The reactor was warmed externally using a water bath. The evolved gas amounts were analyzed using a gas chromatograph (Shimadzu GC-8A) equipped with a thermal conductivity detector and a molecular sieve with 5 Å columns that were directly connected to the closed gas-circulation system. The reaction solution can boil at reduced pressure under illumination or heating, which induces inhomogeneity of the gas components in the closed system and leads to an overestimation of detected gas amounts. To ensure homogeneity of the gas components in the closed system, the reaction solution was sufficiently cooled for each sampling when the temperature was intentionally raised.

To measure the operating potential of the  $\text{CoO}_x/\text{Cr}_2\text{O}_3/\text{Rh}$ -modified LTCA:Mg,Al/Au/BVO:Mo(h) sheet during the ZOWS reaction, the rest potential for the sheet sample was measured in a three-electrode configuration using Ag/AgCl and Pt wire as reference and counter electrodes, respectively.<sup>S7</sup> The electrode potential was converted into reversible hydrogen electrode (RHE) units using Nernst equation. A Cu wire was connected to the Au thin film of the cocatalyst-loaded photocatalyst sheet using indium solder. The Cu wire and indium solder were covered with epoxy resin. A 0.1 M

aqueous solution of Na<sub>2</sub>SO<sub>4</sub> was used as an electrolyte solution while stirring and purging with Ar gas to remove air. The measurements were performed at ambient pressure and temperature.

### **5. Photoelectrochemical measurements:**

The photoelectrochemical properties of the photoelectrodes were investigated in a three-electrode configuration.<sup>S7</sup> The potential of the working photoelectrode was regulated with a potentiostat (Hokuto Denko, HSV-100). A 0.1 M aqueous solution of Na<sub>2</sub>SO<sub>4</sub> was used as an electrolyte solution while stirring and purging with Ar gas unless otherwise noted. In the case of the LTCA:Mg,Al/Au photocathodes, Rh and Cr<sub>2</sub>O<sub>3</sub> cocatalysts were photoelectrochemically deposited from RhCl<sub>3</sub>·3H<sub>2</sub>O and K<sub>2</sub>CrO<sub>4</sub>, respectively, at 0.5 V vs. RHE in a 0.5 M Na<sub>2</sub>SO<sub>4</sub> electrolyte solution under Xe lamp irradiation ( $\lambda > 420$  nm). Electrons from the LTCA photocathode reduced Rh<sup>3+</sup> and Cr<sup>6+</sup> species, while water was oxidized to O<sub>2</sub> at the Pt counter electrode. Note that reaction environments were not completely identical for the sheet and photocathode. However, as long as the cocatalysts are reasonably loaded and exhibit expected functionality, it is possible to investigate the effect of oxide coating. In some cases, TiO<sub>2</sub> (0.3 mg per 3 cm<sup>2</sup>) was deposited onto the photoelectrodes by photodecomposition in a TTIP/H<sub>2</sub>O<sub>2</sub> aqueous solution under visible light irradiation ( $\lambda > 420$  nm) for 2 h. This procedure was conducted in an ambient atmosphere without electrode potential control. Alternatively, SiO<sub>2</sub> (2.7 mg per 3 cm<sup>2</sup>) was manually deposited from TEOS onto the photoelectrodes by hydrolysis.

Current-potential curves were measured at a scan rate of 10 mV s<sup>-1</sup> from negative to positive potential for the LTCA:Mg,Al/Au photocathodes and in the reverse direction for the BVO:Mo/Au photoanodes. The difference in current observed under illumination by visible light ( $\lambda > 420$  nm) from a 300 W Xe lamp and under darkness was attributed to the photocurrent generated by the hydrogen evolution reaction (HER) and the oxygen evolution reaction (OER), respectively, because LTCA photocathodes and BVO photoanodes are known to generate H<sub>2</sub> and O<sub>2</sub> at Faradaic efficiencies close to unity.<sup>S8,S9</sup> To monitor the oxygen reduction reaction (ORR) occurring on the LTCA photocathode, the photocurrent density was measured under visible light ( $\lambda > 420$  nm) from a 300 W Xe lamp in an Ar- and O<sub>2</sub>-purged 0.1 M aqueous Na<sub>2</sub>SO<sub>4</sub> solution (pH 6.7) sequentially using the same electrodes. The potential was changed at a rate of 10 mV s<sup>-1</sup> from positive to negative. The difference in current density observed in the O<sub>2</sub>- and Ar-purged electrolyte solutions was attributed to the ORR current. The Au electrode exhibited identical current-potential profiles under both dark and illuminated conditions.

### **6. Characterization of powdered photocatalysts and sheet samples**

XRD patterns for powdered samples were obtained using a Rigaku MiniFlex 300 powder diffractometer with a Cu K $\alpha$  radiation source ( $\lambda = 1.5418$  Å). UV-vis DRS was performed with a spectrophotometer (V-670, Jasco) equipped with an integrating sphere and a Spectralon standard as a reference for baseline correction. Scanning electron microscopy (Phenom Pharos Desktop SEM, Thermo Scientific) was used to examine the particles shape and size. The elemental distribution, morphology and thickness of the SiO<sub>2</sub> coated sheet samples were determined by spherical aberration corrected high-angle annular dark field scanning transmission electron microscope (Cs-corrected thermal FE-STEM, JEM-ARM200F, JEOL Ltd.). A Cu TEM grid was used for sheet sample, thus strong Cu-K $\alpha$  peak was observed at 8.0 keV in the elemental analysis. LTCA:Mg,Al and BVO:Mo(h) particles were distinguished based on the X-ray peak intensity for La-L $\alpha$  and V-K $\alpha$  at 4.6 and 4.9 keV,

respectively. X-ray photoelectron spectroscopy (XPS) was performed for the sheet samples using a PHI Quantera II spectrometer with an Al K $\alpha$  radiation source. All binding energies were referenced to the C 1s peak (284.8 eV).

### **7. Apparent quantum yield (AQY) measurement:**

The AQY in the ZOWS reaction using a photocatalyst sheet was measured using a similar closed gas circulation system but with different light irradiation wavelength using a monochromatic light source (MAX303, Asahi Spectra Co., Ltd.) The number of incident photons received by the photocatalyst sheet was measured using a grating spectroradiometer (LS-100, EKO Instruments Co., Ltd.). The AQY was calculated using the equation

$$\text{AQY (\%)} = [4 \times R(\text{H}_2) / I] \times 100$$

where  $R(\text{H}_2)$  and  $I$  represent the rate of  $\text{H}_2$  evolution and the number of incident photons, respectively. The total number of incident photons at wavelength 420, 440, 460, 480, 500, 520 and 540 nm were  $2.0 \times 10^{20}$ ,  $2.1 \times 10^{20}$ ,  $2.3 \times 10^{20}$ ,  $2.4 \times 10^{20}$ ,  $1.9 \times 10^{20}$ ,  $2.5 \times 10^{20}$  and  $2.4 \times 10^{20}$  photons  $\text{h}^{-1}$ , respectively, per  $9 \text{ cm}^2$ .

### **8. Solar-to-hydrogen (STH) conversion measurement:**

The STH values in the ZOWS reaction were measured using the same experimental apparatus but under illumination by a solar simulator (HAL-320, Asahi Spectra Co., Ltd.). The STH was calculated as

$$\text{STH (\%)} = (R(\text{H}_2) \times \Delta G_r) / (P \times S) \times 100$$

where  $R(\text{H}_2)$ ,  $\Delta G_r$ ,  $P$ , and  $S$  are the rate of hydrogen gas evolution during Z-scheme OWS, the change in Gibbs free energy that accompanies the water splitting reaction, the energy intensity of the solar light irradiation (AM1.5G), and the irradiation area ( $6.25 \text{ cm}^2$ ), respectively. The energy intensity of the solar light irradiation was nominally  $100 \text{ mW cm}^{-2}$ . A standard Gibbs free energy ( $\Delta G_r$ ) of  $237.13 \text{ kJ mol}^{-1}$  was used for the STH calculation.

## Supplemental Data Items

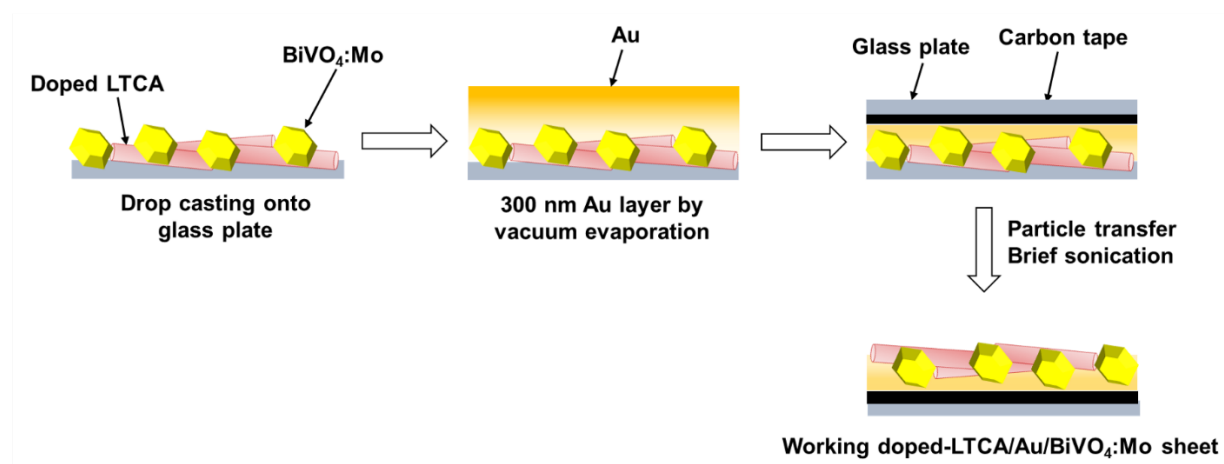


**Figure S1.** Schematic procedure for the fabrication of doped-LTCA/Au/BVO:Mo photocatalyst sheet by particle transfer method.

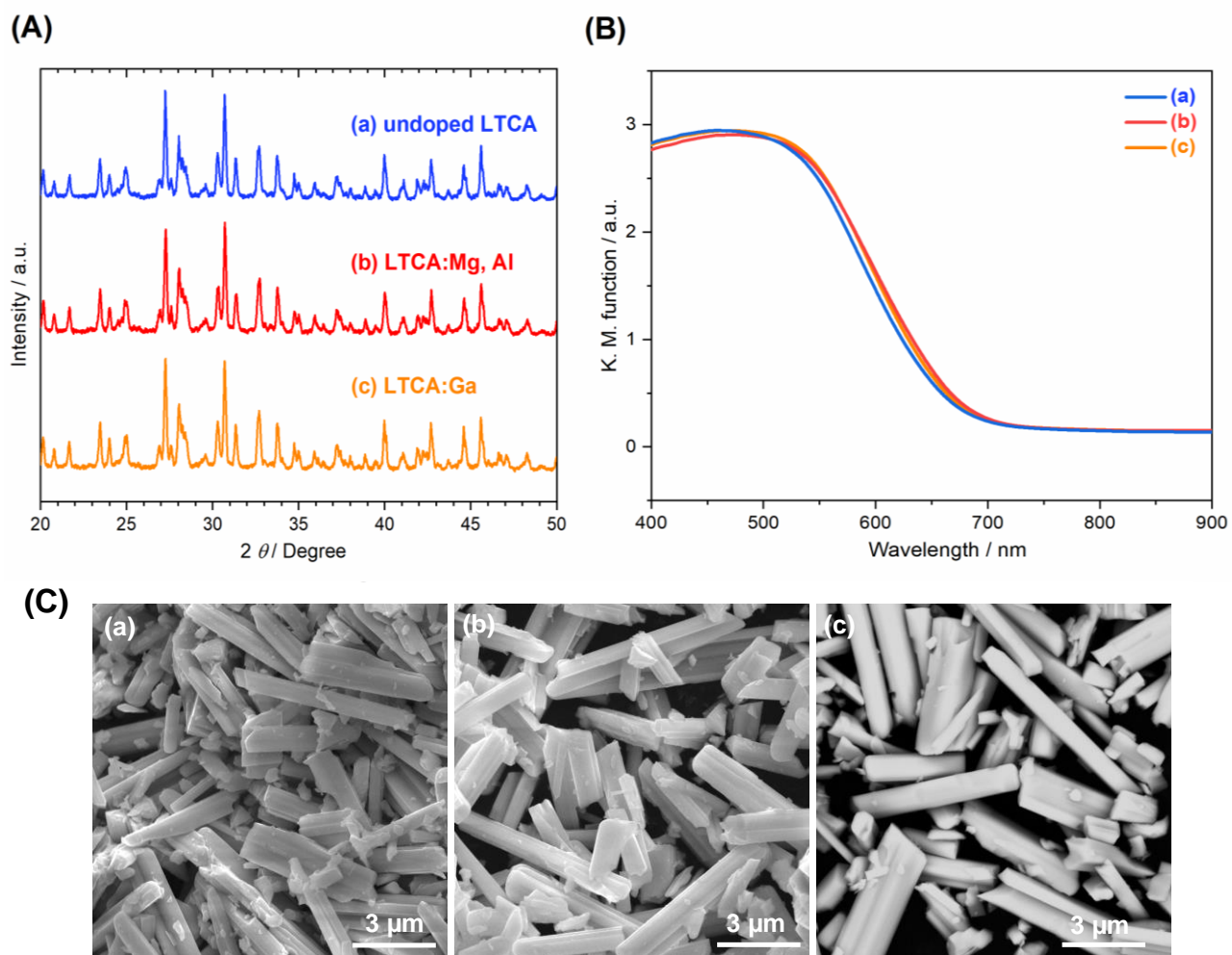


**Figure S2.** (A) XRD patterns, (B) UV-Vis DRS data, and (C) SEM images for (a) undoped LTCA and LTCA (co)-doped with (b) Mg 1% Al 1% and (c) Ga 1%, respectively.

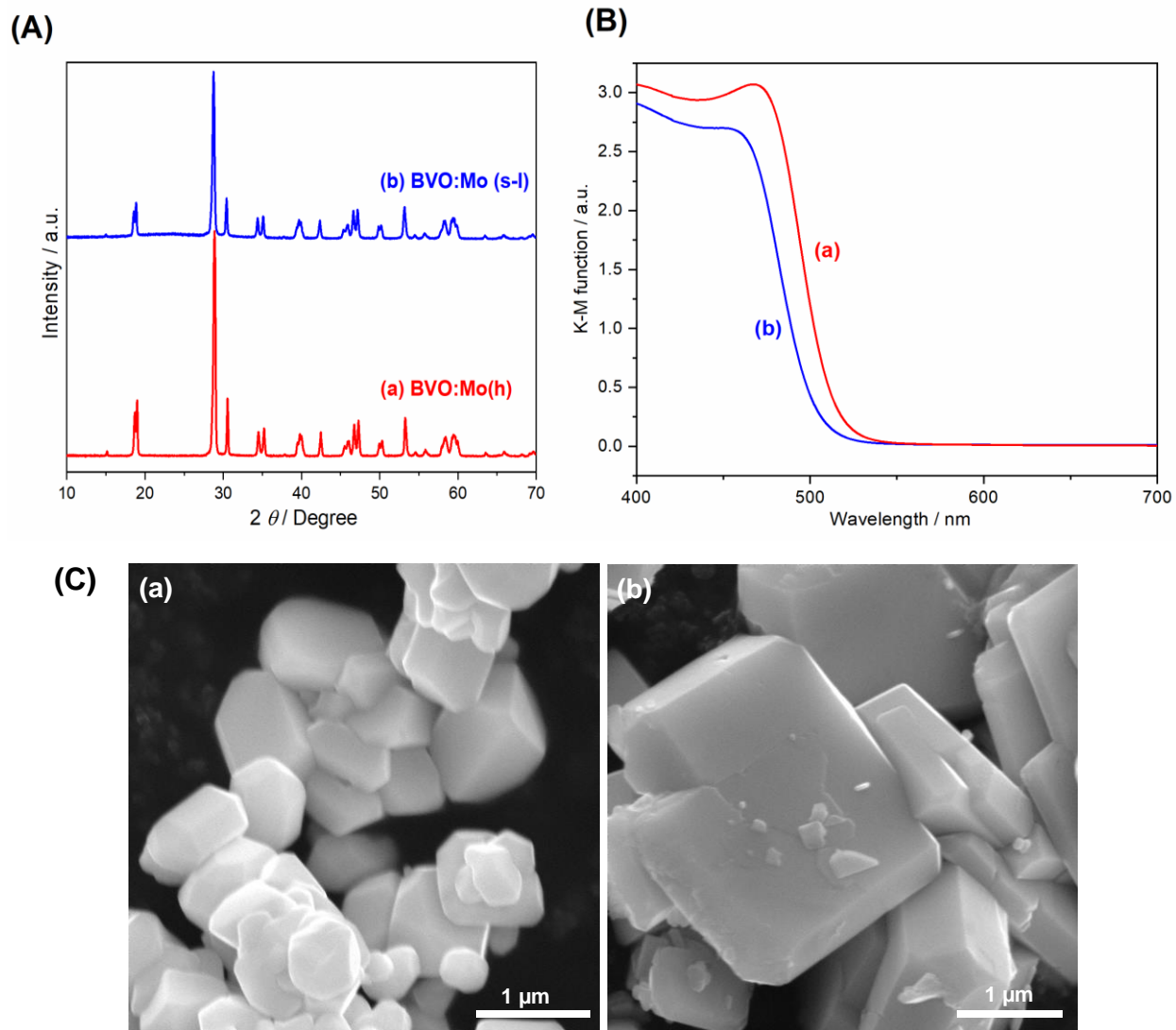


**Figure S3.** (A) XRD patterns, (B) UV-Vis DRS data, and (C) SEM images of Mo-doped  $\text{BiVO}_4$  synthesized by (a) hydrothermal and (b) solid-liquid reaction methods, respectively.

**Table S1.** ZOWS activities of photocatalyst sheets (9 cm<sup>2</sup>) employing LTCA:*M* (*M*= dopants), BVO:Mo(h) and BVO:Mo(s-l) photocatalysts with underlying Au back contact layer.

LTCA: <i>M</i> (HEP)	BiVO <sub>4</sub> :Mo (OEP)	<i>r</i> <sub>H<sub>2</sub></sub> (μmol/h)	<i>r</i> <sub>O<sub>2</sub></sub> (μmol/h)
Ga	s-l	68	33
	hyd	82	40
Mg, Al	s-l	90	45
	hyd	111	55

**Reaction conditions:** photocatalysts 10 mg each; 40 mL ultrapure water; cocatalysts CoO<sub>x</sub>/Cr<sub>2</sub>O<sub>3</sub>/Rh where 0.1 μmol Rh, 0.2 μmol Cr and 0.05 μmol Co were used; light source 300 W Xe lamp equipped with a cut-off filter (λ > 420 nm).

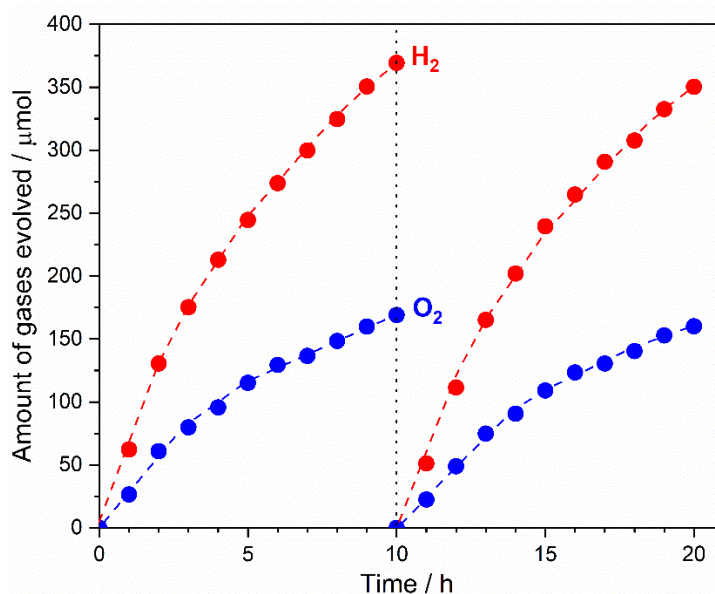


**Figure S4.** Long-term stability measurement of CoO<sub>x</sub>/Cr<sub>2</sub>O<sub>3</sub>/Rh-loaded LTCA:Mg,Al/Au/BVO:Mo(h) photocatalyst sheet at background pressure 10 kPa and temperature 283 K under visible light (λ > 420 nm).

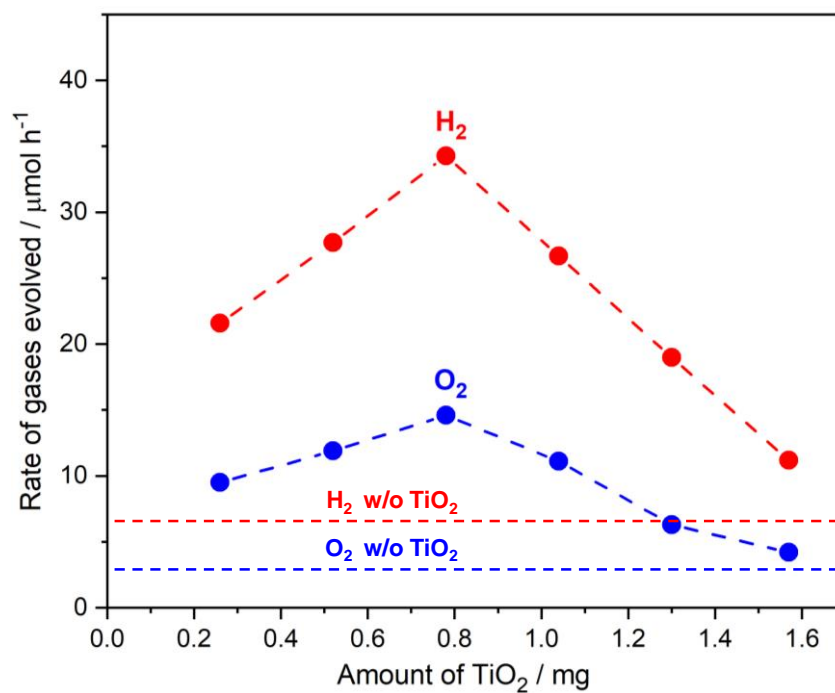


**Figure S5.** ZOWS activity of CoO<sub>x</sub>/Cr<sub>2</sub>O<sub>3</sub>/Rh-coated LTCA:Mg,Al/Au/BVO:Mo photocatalyst sheets modified with varying amounts (0.26-1.6 mg) of amorphous TiO<sub>2</sub> layer under visible light ( $\lambda > 420$  nm) irradiation from a 300 W Xe lamp at initial background pressure of 90 kPa and temperature of 283 K.

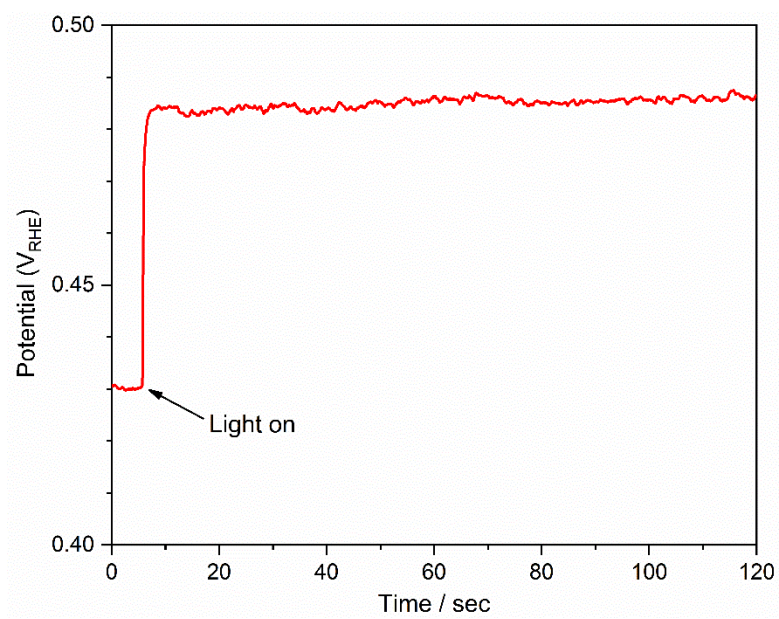


**Figure S6.** Rest potential of CoO<sub>x</sub>/Cr<sub>2</sub>O<sub>3</sub>/Rh-loaded LTCA:Mg,Al/Au/BVO:Mo(h) photocatalyst sheet in 100 mL 0.1 M Na<sub>2</sub>SO<sub>4</sub> aqueous solution under visible light ( $\lambda > 420$  nm) from 300 W Xe lamp.

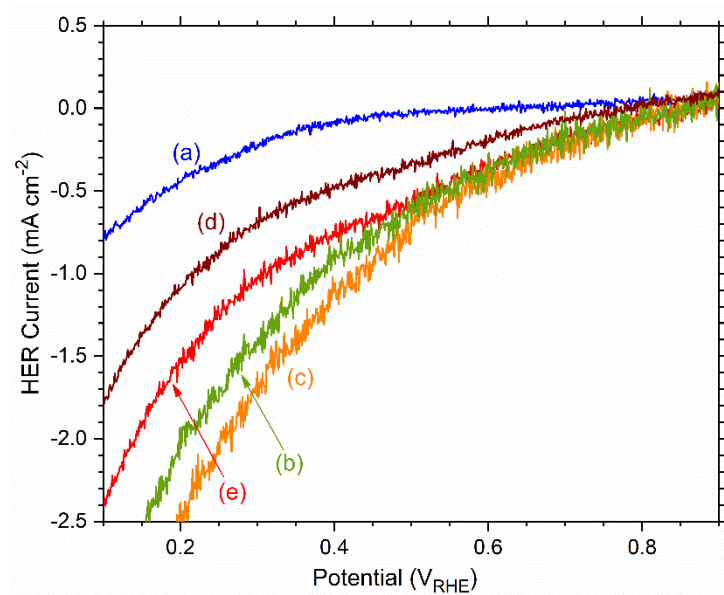


**Figure S7.** Current-potential curves for (a) unmodified LTCA:Mg,Al/Au, (b) Rh/LTCA:Mg,Al/Au, (c) Cr<sub>2</sub>O<sub>3</sub>/Rh/LTCA:Mg,Al/Au, (d) TiO<sub>2</sub>/Cr<sub>2</sub>O<sub>3</sub>/Rh/LTCA:Mg,Al/Au and (e) SiO<sub>2</sub>/Cr<sub>2</sub>O<sub>3</sub>/Rh/LTCA:Mg,Al/Au photocathodes in Ar saturated 0.1 M Na<sub>2</sub>SO<sub>4</sub> (pH 6.7) electrolyte solution under visible light ( $\lambda > 420$  nm) irradiation from 300 W Xe lamp.

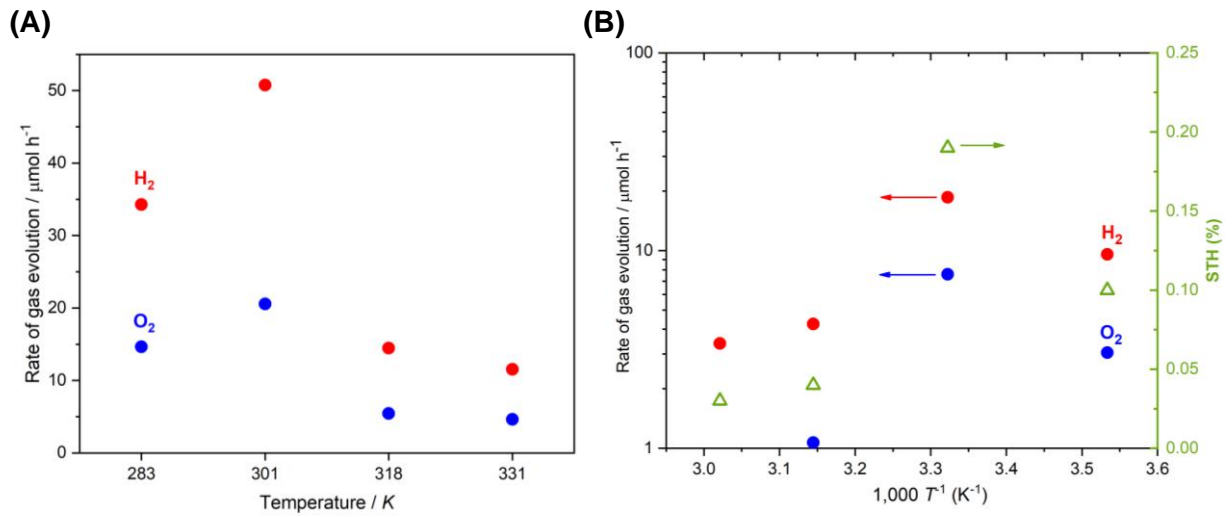


**Figure S8.** Temperature ( $T$ ) dependence of ZOWS activity for  $\text{TiO}_2$  (0.8 mg)-modified  $\text{CoO}_x/\text{Cr}_2\text{O}_3/\text{Rh}$ -loaded LTCA:Mg,Al/BVO:Mo photocatalyst sheet ( $9 \text{ cm}^2$ ) at initial background pressure of 90 kPa under (A) visible light ( $\lambda > 420 \text{ nm}$ ) irradiation from 300 W Xe lamp and (B) simulated sunlight AM 1.5G along with STH values (green triangles).

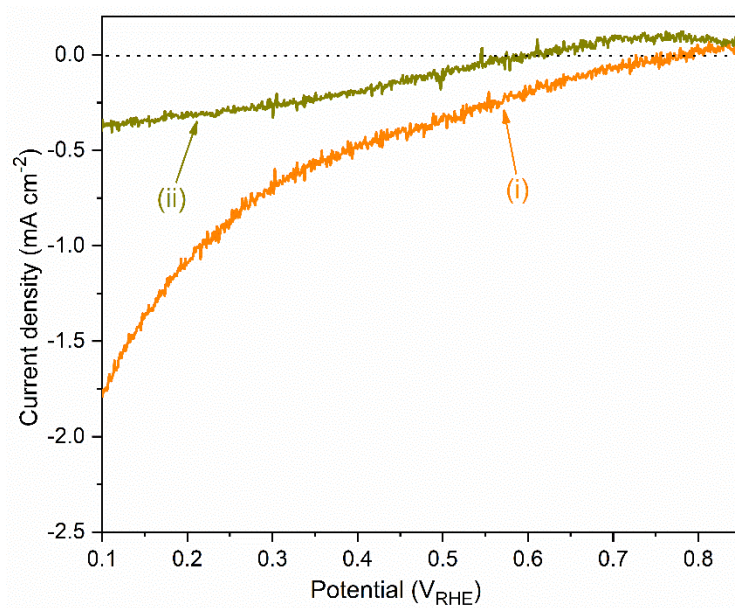


**Figure S9.** Current-potential curves for amorphous TiO<sub>2</sub> modified Cr<sub>2</sub>O<sub>3</sub>/Rh-loaded LTCA:Mg,Al/Au photocathode (i) before and (ii) after heat treatment at 318 K in water. Reaction conditions: 0.1 M Na<sub>2</sub>SO<sub>4</sub> (pH 6.7) electrolyte solution saturated with Ar under visible light irradiation ( $\lambda > 420$  nm) by a 300 W Xe lamp.

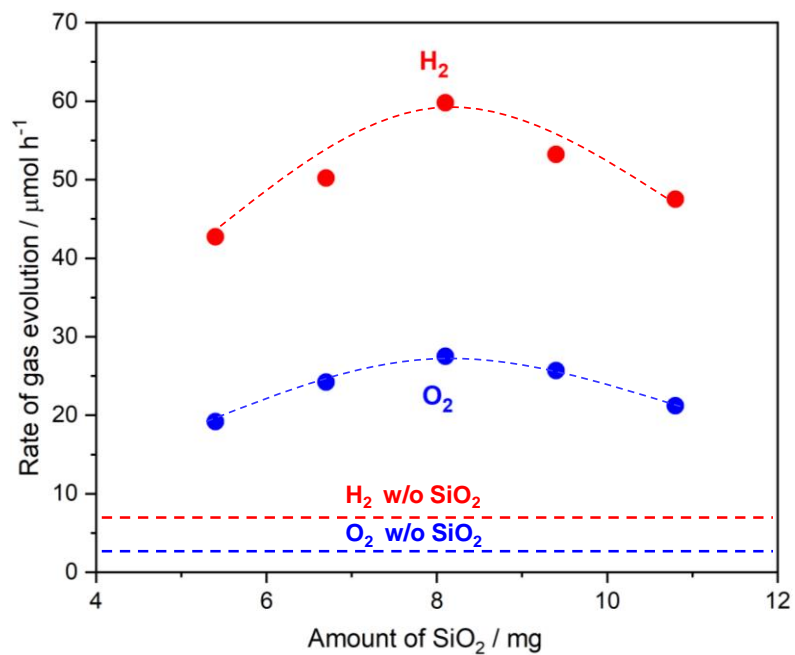


**Figure S10.** ZOWS activity of  $\text{CoO}_x/\text{Cr}_2\text{O}_3/\text{Rh}$ -coloaded  $\text{LTCA}:\text{Mg,Al/Au/BVO}:\text{Mo}$  photocatalyst sheet ( $9 \text{ cm}^2$ ) modified with varying amounts (5.4-10.8 mg) of amorphous  $\text{SiO}_2$  at initial background pressure of 90 kPa and temperature of 283 K under visible light ( $\lambda > 420 \text{ nm}$ ) irradiation by a 300 W Xe lamp.

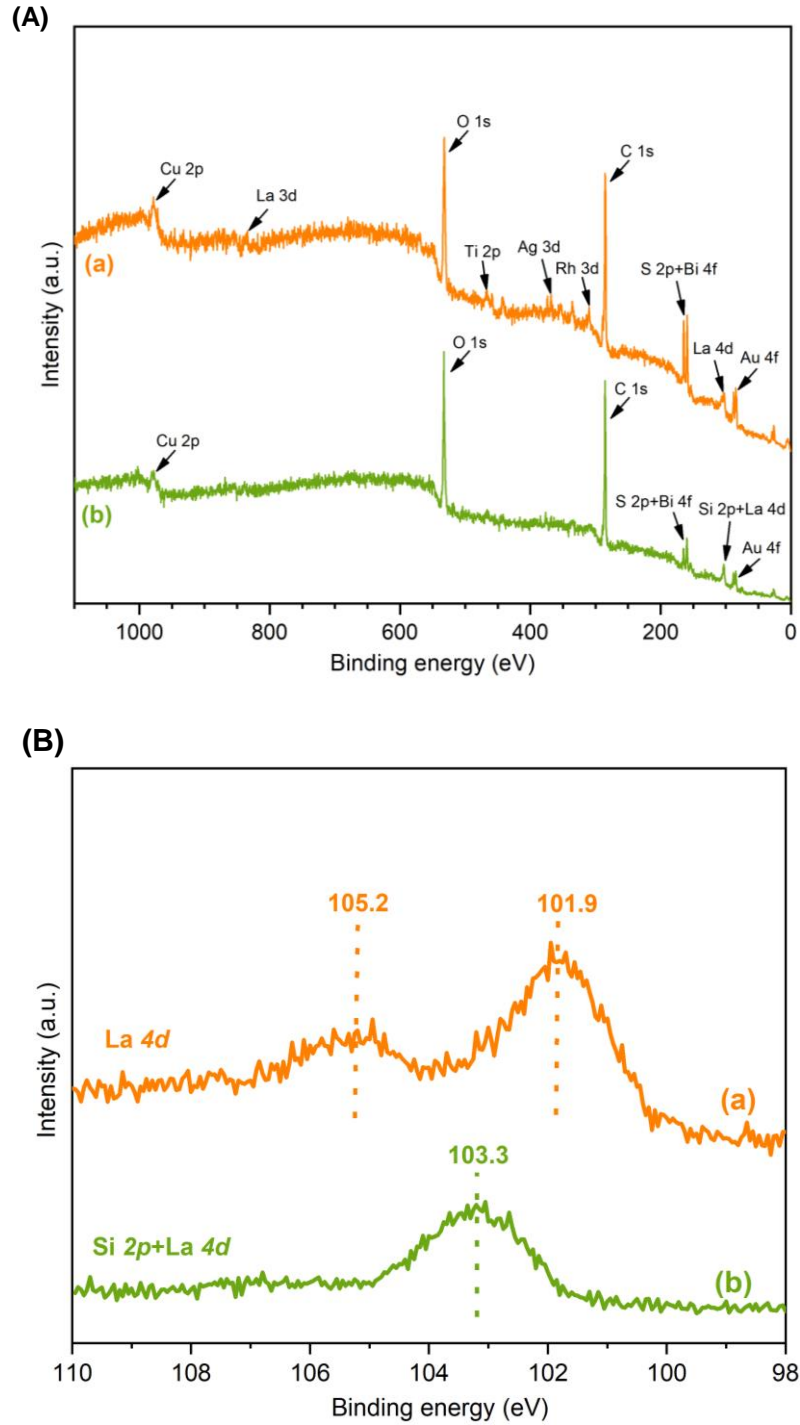


**Figure S11.** (A) Wide- and (B) narrow-scan XPS spectra for  $\text{CoO}_x/\text{Cr}_2\text{O}_3/\text{Rh}$  cocatalyst-loaded LTCA:Mg,Al/Au/BVO:Mo(h) photocatalyst sheets (a) without and (b) with  $\text{SiO}_2$  coating. From panel (B), it can be seen that the La 4d and Si 2p binding energies are close to each other. Surface modification of the sheet with  $\text{SiO}_2$  suppressed the La 4d peak intensity, which indicates that the  $\text{SiO}_2$  layer covered the LTCA:Mg,Al surface to prevent the ORR backward reaction.

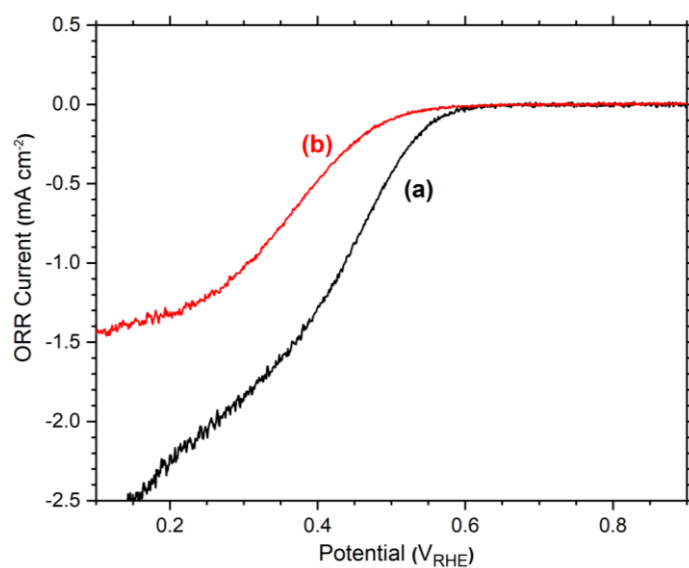


**Figure S12.** Oxygen reduction current density for (a) bare Au/Ti, (b) SiO<sub>2</sub>-modified Au/Ti electrodes. Reaction conditions: 0.1 M Na<sub>2</sub>SO<sub>4</sub> (pH 6.7) electrolyte solution saturated with O<sub>2</sub> (for ORR) or Ar (for HER) under visible light irradiation ( $\lambda > 420$  nm) from a 300 W Xe lamp.

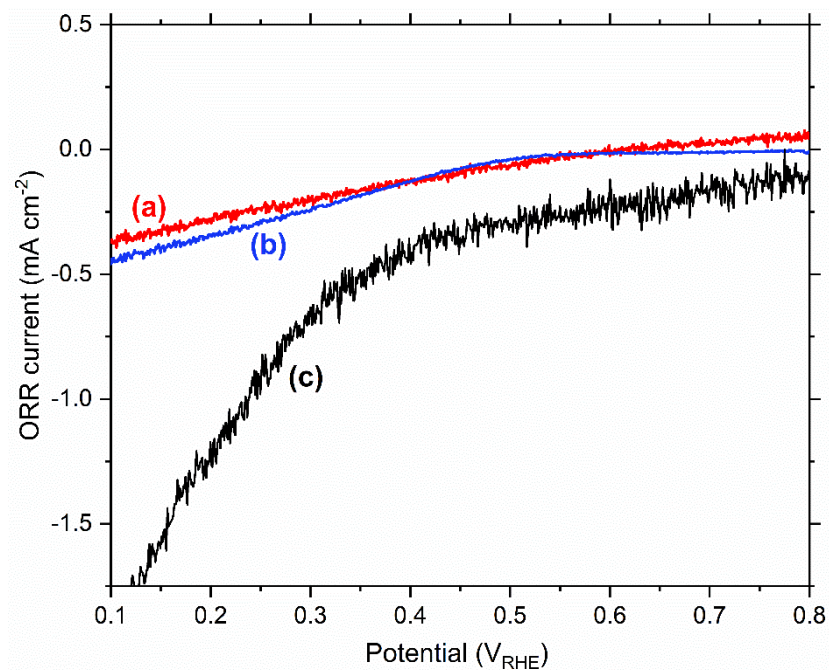


**Figure S13.** ORR current-potential curves for SiO<sub>2</sub>/Cr<sub>2</sub>O<sub>3</sub>/Rh/LTCA:Mg,Al/Au photoelectrodes (a) before, (b) after heat treatment (at 333 K) in 0.1 M Na<sub>2</sub>SO<sub>4</sub> (pH 6.7) electrolyte solution under visible light ( $\lambda > 420$  nm). (c) Results for Cr<sub>2</sub>O<sub>3</sub>/Rh/LTCA:Mg,Al/Au photoelectrode shown as reference.

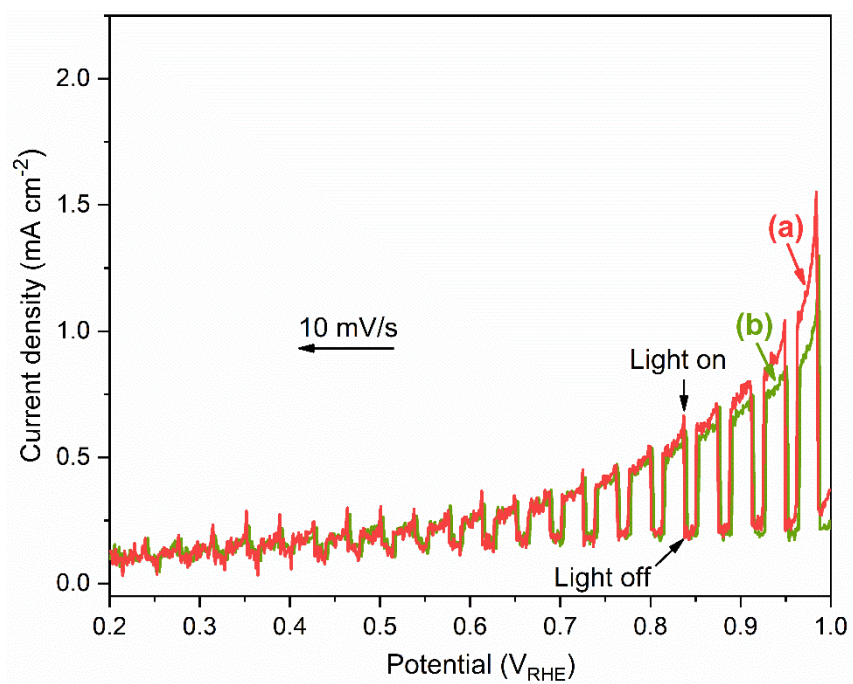


**Figure S14.** Current-potential curves for (a) BVO:Mo(h)/Au and (b) SiO<sub>2</sub>/BVO:Mo(h)/Au photoanodes in Ar saturated 0.1 M Na<sub>2</sub>SO<sub>4</sub> (pH 6.7) electrolyte solution under visible light ( $\lambda > 420$  nm).

**Table S2.** STH efficiencies of CoO<sub>x</sub>/Cr<sub>2</sub>O<sub>3</sub>/Rh/LTCA:Mg,Al/Au/BVO:Mo(h) sheets optimally modified with TiO<sub>2</sub> or SiO<sub>2</sub> at various temperatures.

Temperature /K	Coating layer	$r_{H_2}$ ( $\mu\text{mol/h}$ )	$r_{O_2}$ ( $\mu\text{mol/h}$ )	STH (%)
283	TiO <sub>2</sub>	10	3	0.11
	SiO <sub>2</sub>	23	10	0.24
301	TiO <sub>2</sub>	19	7	0.19
	SiO <sub>2</sub>	30	13	0.32
318	TiO <sub>2</sub>	4	1	0.04
	SiO <sub>2</sub>	35	14	0.37
333	TiO <sub>2</sub>	3	<i>n.d.</i>	0.03
	SiO <sub>2</sub>	38	17	<b>0.41</b>

\**n.d.* : not detected

**Reaction conditions:** Coating layer TiO<sub>2</sub> (0.8 mg/9 cm<sup>2</sup>) or SiO<sub>2</sub> (8.1 mg/9 cm<sup>2</sup>); light source simulated sunlight AM 1.5G.

**Table S3.** Representative Z-scheme OWS systems employing non-oxide photocatalysts as HEP and/or OEP along with their efficiencies.

Entry	Cocatalyst/HEP (Absorption edge)	Cocatalyst/OEP (Absorption edge)	Mediator	System Type	AQY (Wavelength/nm)	STH (Pressure, Temperature)	Refs
1	Rh <sub>y</sub> Cr <sub>2-2y</sub> O <sub>3</sub> -ZrO <sub>2</sub> /TaON (520 nm)	Au/CoO <sub>x</sub> /BiVO <sub>4</sub> (h) (520 nm)	Fe(CN) <sub>6</sub> <sup>3-/4-</sup>	Suspension	10.3% (420 nm)	0.5% (298 K) <sup>a</sup>	S2
2	Pt/BaTaO <sub>2</sub> N (660 nm)	PtO <sub>x</sub> /WO <sub>3</sub> (430 nm)	IO <sub>3</sub> <sup>-</sup> /I <sup>-</sup>	Suspension	4.0% (420 nm)	0.24% (288 K) <sup>a</sup>	S10
3	Pt/ZnIn <sub>2</sub> S <sub>4</sub> (630 nm)	CoO <sub>x</sub> /WO <sub>3</sub> (430 nm)	C-wood	Suspension	21.6% (380 nm)	1.52% <sup>a</sup>	S11
4	ZrO <sub>2</sub> /TaON (525 nm)	Ir-FeCoO <sub>x</sub> /BiVO <sub>4</sub> (h) (530 nm)	Fe(CN) <sub>6</sub> <sup>3-/4-</sup>	Suspension	12.3% (420 nm)	0.6% <sup>a</sup>	S12
5	Pt-MgTa <sub>2</sub> O <sub>6-x</sub> N <sub>y</sub> /TaON (550 nm)	PtO <sub>x</sub> /WO <sub>3</sub> (450 nm)	IO <sub>3</sub> <sup>-</sup> /I <sup>-</sup>	Suspension	6.8% (420 nm)	---	S13
6	Pt/(CuGa) <sub>0.5</sub> ZnS <sub>2</sub> (560 nm)	CoO <sub>x</sub> /BiVO <sub>4</sub> (520 nm)	RGO	Suspension	0.80% (440 nm)	0.024% <sup>a</sup>	S14
7	Pt/NiS/La <sub>5</sub> Ti <sub>2</sub> AgS <sub>5</sub> O <sub>7</sub> (570 nm)	PtO <sub>x</sub> /(H <sup>+</sup> ,Cs <sup>+</sup> )WO <sub>3</sub> (440 nm)	I <sub>3</sub> <sup>-</sup> /I <sup>-</sup>	Suspension	0.12% (420 nm)	---	S15
8	Pt/TiO <sub>2</sub> -CdS- (ZnSe) <sub>0.5</sub> (CuGa <sub>2.5</sub> Se <sub>4.25</sub> ) <sub>0.5</sub> (725 nm)	BiVO <sub>4</sub> :Mo(s-l) (520 nm)	Au	Sheet	1.5% (420 nm)	---	S16
9	RhCrO <sub>x</sub> /LaMg <sub>1/3</sub> Ta <sub>2/3</sub> O <sub>2</sub> N (600nm)	BiVO <sub>4</sub> :Mo (520 nm)	Au and RGO	Sheet	0.25% (418 nm)	0.0035% <sup>a</sup>	S17
10	Rh/Cr <sub>2</sub> O <sub>3</sub> /LTCA:Ga (700 nm)	CoO <sub>x</sub> /LaTiO <sub>2</sub> N (600 nm)	Au	Sheet	0.04% (420 nm)	---	S18
11	Cr <sub>2</sub> O <sub>3</sub> /Rh/LTCA:Ga (700 nm)	CoO <sub>x</sub> /BiVO <sub>4</sub> :Mo(s-l) (520 nm)	Au	Sheet	11.8% (420 nm)	0.4% (4 kPa, 301 K)	S5
12	Cr <sub>2</sub> O <sub>3</sub> /Rh/LTCA:Mg,Al (700 nm)	CoO <sub>x</sub> /BiVO <sub>4</sub> :Mo(h) (520 nm)	Au	Sheet	<b>16.3%</b> (420 nm)	<b>0.67%</b> (4 kPa, 301 K)	This work
13	SiO <sub>2</sub> /Cr <sub>2</sub> O <sub>3</sub> /Rh/LTCA:Mg,Al (700 nm)	SiO <sub>2</sub> /CoO <sub>x</sub> /BiVO <sub>4</sub> :Mo(h) (520 nm)	Au	Sheet	<b>9.7%</b> (420 nm)	<b>0.41%</b> (90 kPa, 333 K)	This work

<sup>a</sup> Background pressure was not specified, likely recorded under reduced pressure.

## Supplemental References:

- S1. Sun, S., et al. (2018). Efficient redox-mediator-free Z-scheme water splitting employing oxysulfide photocatalysts under visible light. *ACS Catal.* *8*, 1690–1696.
- S2. Qi, Y., et al. (2018). Redox-Based Visible-Light-Driven Z-Scheme Overall water splitting with apparent quantum efficiency exceeding 10%. *Joule.* *2*, 2393–2402.
- S3. Wang, Q., et al. (2016). Scalable water splitting on particulate photocatalyst sheets with a solar-to-hydrogen energy conversion efficiency exceeding 1%. *Nat. Mater.* *15*, 611–615.
- S4. Hisatomi, T., et al. (2015).  $\text{La}_5\text{Ti}_2\text{Cu}_{1-x}\text{Ag}_x\text{S}_5\text{O}_7$  photocathodes operating at positive potentials during photoelectrochemical hydrogen evolution under irradiation of up to 710 nm. *Energy Environ. Sci.* *8*, 3354–3362.
- S5. Chen, S., Nandy, S., et al. (2023). Promotion of charge carriers utilization over  $\text{La}_5\text{Ti}_2\text{Cu}_{0.9}\text{Ag}_{0.1}\text{O}_7\text{S}_5$ -based photocatalyst sheet for efficient Z-scheme overall water splitting. *ACS Catal.* *13*, 3285–3294.
- S6. Pan, C., et al. (2015). A complex perovskite-type oxynitride: the first photocatalyst for water splitting operable at up to 600 nm. *Angew. Chem. Int. Ed.* *54*, 2955–2959.
- S7. Jang, J. W., et al. (2015). Enabling unassisted solar water splitting by iron oxide and silicon. *Nat. Commun.* *6*, 7447.
- S8. Ma, G., et al. (2015). Photoanodic and photocathodic behaviour of  $\text{La}_5\text{Ti}_2\text{CuS}_5\text{O}_7$  electrodes in the water splitting reaction. *Chem. Sci.* *6*, 4513–4518.
- S9. Zhong, M., et al. (2015). Surface modification of  $\text{CoO}_x$  loaded  $\text{BiVO}_4$  photoanodes with ultrathin p-type NiO layers for improved solar water oxidation. *J. Am. Chem. Soc.* *137*, 5053–5060.
- S10. Wang, Z., et al. (2021). Sequential cocatalyst decoration on  $\text{BaTaO}_2\text{N}$  towards highly-active Z-scheme water splitting. *Nat. Commun.* *12*, 1005.
- S11. Wang, Y., et al. (2021). Sulfur-Deficient  $\text{ZnIn}_2\text{S}_4$ /Oxygen-Deficient  $\text{WO}_3$  Hybrids with Carbon Layer Bridges as a Novel Photothermal/ Photocatalytic Integrated System for Z-Scheme Overall Water Splitting. *Adv. Energy Mater.* *11*, 2102452.
- S12. Qi, Y., et al. (2022). Unraveling of cocatalysts photodeposited selectively on facets of  $\text{BiVO}_4$  to boost solar water splitting. *Nat. Commun.* *13*, 484.
- S13. Chen, S., et al. (2015) Efficient visible-light-driven Z-scheme overall water splitting using a  $\text{MgTa}_2\text{O}_{6-x}\text{N}_y/\text{TaON}$  heterostructure photocatalyst for  $\text{H}_2$  evolution. *Angew. Chem. Int. Ed.* *54*, 8498–8501.
- S14. Yoshino, S., et al. (2020). Z-schematic solar water splitting using fine particles of  $\text{H}_2$ -evolving  $(\text{CuGa})_{0.5}\text{ZnS}_2$  photocatalyst prepared by a flux method with chloride salts. *ACS Appl. Energy Mater.* *3*, 5684–5692.
- S15. Song, Z., et al. (2019). Visible-Light-Driven Photocatalytic Z-Scheme Overall Water Splitting in  $\text{La}_5\text{Ti}_2\text{AgS}_5\text{O}_7$ -based Powder-Suspension System. *ChemSusChem* *12*, 1906–1910.
- S16. Chen, S., et al. (2021). Surface modifications of  $(\text{ZnSe})_{0.5}(\text{CuGa}_{2.5}\text{Se}_{4.25})_{0.5}$  to promote photocatalytic Z-scheme overall water splitting. *J. Am. Chem. Soc.* *143*, 10633–10641.
- S17. Pan, Z., et al. (2016) Photoreduced graphene oxide as a conductive binder to improve the water splitting activity of photocatalyst sheets. *Adv. Funct. Mater.* *26*, 7011–7019.
- S18. Hisatomi, T., et al. (2018). Particulate photocatalyst sheets based on non-oxide semiconductor materials for water splitting under visible light irradiation. *Catal. Sci. Technol.* *8*, 3918–3925.